# High-resolution optical microscopy in complex environments with a single-pixel detector

**Tianshun Zhang,[1] Yang Peng,[1] and Wen Chen[1,2,a)]**

**AFFILIATIONS**

[1]Department of Electrical and Electronic Engineering, The Hong Kong Polytechnic University, Hong Kong, China

[2]Photonics Research Institute, The Hong Kong Polytechnic University, Hong Kong, China

[a)]**Author to whom correspondence should be addressed:** owen.chen@polyu.edu.hk

**ABSTRACT**

Optical microscopy faces a challenge in strongly scattering environments due to severe light attenuations and wave degradations. Here, we report high-resolution optical microscopy in complex environments with a single-pixel detector. By projecting miniaturized random patterns onto a specimen, a series of light intensities can be synchronously collected via single-pixel detection. Dynamic variations of the turbidity in complex scattering environments induce nonlinear attenuations. A framework of untrained neural networks (UNN) enhanced by a physical model is developed to estimate a series of scattering-induced scaling factors and achieve high-resolution object reconstruction. The designed optical microscopy system, employing a tunable lens with autofocusing, is also applied to reconstruct high-quality and high-resolution images of biological specimens over the varying fields of view (FOVs) against complex and dynamic scattering. It is demonstrated in experiments that the proposed method is effective and robust, providing a viable approach for optical microscopy through complex scattering in dynamic media.

Optical microscopy in complex scattering environments has been well recognized as a challenge. Scattering media could induce severe distortions that disrupt inherent point-to-pixel correspondence, substantially degrading spatial resolution and image quality. Although advanced techniques have been proposed (e.g., NIR-II fluorescence imaging,[1] self-reconstructing beams[2] and optical memory effect[3]), these methods could have the limitations, e.g., limited penetration depth and sophisticated hardware. Single-pixel microscopy,[4–11] leveraging computational imaging via single-pixel detection, offers advantages like scattering resistance, cost-effective devices, high light sensitivity, and wide operational bandwidth etc. Previous work[12] demonstrated its potential through thick scattering media. However, existing studies rely predominantly on specialized structured illumination patterns (e.g., Fourier or Hadamard basis[13]) with orthogonal completeness to ensure satisfactory image quality. Although random illumination patterns have been explored in *prior* studies,[14–19] the implementations achieve only low-quality reconstruction of simple and binary objects, and it is considered to be insufficient for high-resolution bioimaging in microscopy.

Ghost imaging (GI) with random illumination patterns proves to be ineffective in dynamic scattering environments with time-varying turbidity, where nonlinear scaling factors disrupt the measurements. Advanced correction strategies[20–23] targeting nonlinear scaling factors partially mitigate scattering effects but yield suboptimal reconstruction quality, necessitating enhanced approaches. Deep learning has gained much attention in optical microscopy for resolution enhancement,[24,25] autofocusing,[26,27] and aberration correction,[28,29] while also emerging as a powerful tool in single-pixel imaging.[30] Data-driven implementations[31] require extensive labeled datasets for training. They are prohibitively difficult to obtain in complex scattering scenarios where high-quality ground truths and scattering information remain elusive. Practical deployment is further constrained by limited generalizability and interpretability challenges.[32] Physics-enhanced untrained neural networks (UNN)[33–35] address these constraints by demonstrating robust anti-interference capabilities and enabling high-quality reconstructions without training. Nevertheless, an investigation of their performance for single-pixel microscopy through dynamic and complex scattering media remains unexplored.

In this Letter, we report a framework integrating a physical model with UNN to achieve high-resolution single-pixel optical microscopy through complex scattering media. Random illumination patterns are directly employed without a special design. By integrating a tunable lens with autofocusing, high-quality object reconstructions are realized over the varying fields of view (FOVs). The proposed framework effectively eliminates dynamic scaling factors without any datasets. Experimental results demonstrate high robustness against scattering, and exhibit high effectiveness for biological imaging. Our method can provide a promising solution for high-resolution optical microscopic imaging in harsh environments.

A schematic experimental setup for single-pixel microscopy through complex scattering media is shown in Fig. 1. A green laser (maximum power of 200 mW, wavelength of 532 nm) is used to

illuminate a digital micro-mirror device (DMD, Texas Instruments) with pixel size of 10.8 μm at 24.0°. Random binary patterns are sequentially displayed by DMD. The reflected waves propagate through a 4*f* system (plano-convex lens and tube lens with the same focal length of 20 cm). An iris is used to allow only zero-order light to enter the objective lens (NA of 0.55 and 50× Mitutoyo), filtering out excess diffraction orders. An electronically-controlled tunable lens (Optotune-EL-12-30-TC), in conjunction with the objective lens, is applied to focus miniaturized patterns onto an object over the varying FOVs. A water tank (polymethyl methacrylate) with a dimension of 5.0 cm (length) × 10.0 cm (width) × 30.0 cm (height) filled with 1000.0-ml clean water is placed close to the object. A turbulent scattering environment with time-varying turbidity is created via dripping milk emulsion (5.0-ml skimmed milk mixed with 200.0-ml clean water) into the tank while a motor-driven stirrer was kept agitating the liquid at 450 rpm. A Fresnel lens (a diameter of 30.0 cm and a focal length of 12.0 cm) collects the scattered light, and a series of focused light intensities are sequentially detected by a single-pixel silicon photodiode (SPD, PDA100A2 Thorlabs).

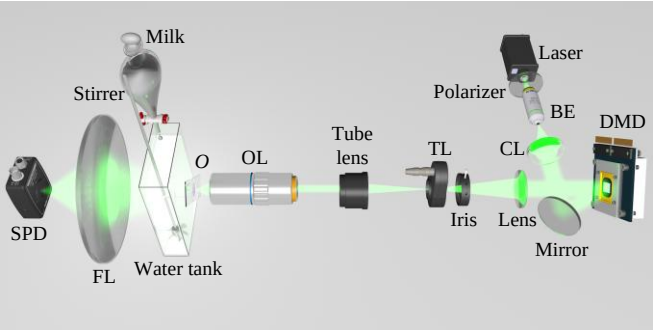


**FIG. 1.** A schematic experimental setup for the developed single-pixel optical microscopy through complex scattering media. *O*: object; BE: beam expander; CL: collimating lens; TL: tunable lens; OL: objective lens; FL: Fresnel lens; SPD: single-pixel silicon photodiode.

When random patterns are adopted for the illumination (e.g., differential GI (DGI)[36]), an object image can be reconstructed via second-order correlation. When complex and dynamic scattering exists in the optical path, a series of dynamic scaling factors could be induced, leading to a mismatch between illumination patterns and the measurements. The measurements $\tilde{B}_i$ can be described by

$$\tilde{B}_i = k_i \iint P_i(\mathrm{x},\mathrm{y}) O(\mathrm{x},\mathrm{y}) d\mathrm{x}d\mathrm{y}, \tag{1}$$

where $i = 1, 2, 3 \cdots, N$, $N$ denotes the total measurement number, $k_i$ denotes a scaling factor, $P_i(\mathrm{x},\mathrm{y})$ denotes random binary patterns, and $O(\mathrm{x},\mathrm{y})$ denotes an object.

As an ill-posed inverse problem, the removal of heterogeneous scaling factors in UNN requires an optimization enhanced by a physical model. Figure 2 shows the proposed strategy with dual U-Net. The architecture in each neural network comprises an autoencoder incorporating skip connections.[37] The inputs of the framework consist of binary random patterns $P$ and the measurements $\tilde{B}$. The U-Net $\mathrm{F}_o$ with a $\sqrt{N} \times \sqrt{N}$ random grayscale input $z_o$ is designed and applied to estimate an object image $\hat{O}$ with $\sqrt{N} \times \sqrt{N}$ pixels. Here, single-pixel imaging principle is embedded to generate a series of corrected measurements $B$ via a single convolutional layer. Each convolution kernel is designed by using a random pattern $P_i(\mathrm{x},\mathrm{y})$ whose pixels serve as weights of the kernels, and the total number of channels is equivalent to that of random patterns. The series of corrected measurements $B$ can be described by

$$B_i = \iint P_i(\mathrm{x},\mathrm{y}) \mathrm{F}_o(z_o) d\mathrm{x}d\mathrm{y}, \tag{2}$$

where $\mathrm{F}_o(z_o)$ denotes an output of neural network $\mathrm{F}_o$, i.e., $\hat{O}$ in Fig. 2. The designed GI-based physical model can represent a relationship between random binary patterns and corrected measurements. The correlation between illumination patterns and corrected measurements is established to show the imaging process without scattering media. Therefore, with a series of single-pixel intensity measurements, the inverse problem can be well defined.

In Fig. 2, U-Net $\mathrm{F}_k$ is designed to estimate a series of scaling factors, employing an initialization strategy analogous to that used in neural network $\mathrm{F}_o$. The predicted 2D scaling factor map $K$ with $\sqrt{N} \times \sqrt{N}$ pixels is flattened to a 1D vector $\hat{K}$. The estimated measurements $\hat{B}$ through complex scattering media can be obtained by

$$\hat{B} = \hat{K} \bullet B, \tag{3}$$

where $\bullet$ denotes Hadamard product. The neural networks operate in parallel to be optimized via a loss function described by

$$\min_{\mathrm{F}_o, \mathrm{F}_k} \left\| \hat{B} - \tilde{B} \right\|^2. \tag{4}$$

The designed dual-UNN framework has a unified structure, and a joint optimization operation could facilitate the convergence.[37] The Adam optimizer with a learning rate of 0.001 is used to update the parameters of neural networks $\mathrm{F}_o$ and $\mathrm{F}_k$ based on NVIDIA GeForce RTX 4090 GPU. The framework is implemented in PyTorch without datasets or labeled data. After optimization, optimal configurations can be obtained, ultimately producing a high-quality object image and a series of dynamic scaling factors, i.e., as the outputs of the designed framework. The proposed framework is validated to be robust against noise via optical experiments.

To realize high-resolution single-pixel microscopic imaging through complex media, it is important to know accurate focal positions. There are several methods for autofocusing.[38–41] Here, the focal position is determined through the total power curve of Fourier power spectrum acquired by Fourier single-pixel imaging.[38] The total power is calculated via the sum of a few coefficients (i.e., indicated by red circles with a radius of 10 pixels) in Fourier power spectrum (64×64 pixels), as typically shown in Fig. 3(a). Varied powers can be observed by adjusting the focal power, i.e., diopter (dpt), of the tunable lens in Fig. 1. Then, a fitting

curve can be determined, and its peak indicates the focal position. For instance, the focal position is determined by identifying the maximum power of 3.11 corresponding to the focal power of 3.56 dpt in Fig. 3(a). It is worth noting that focal positions would be different, when different FOVs are applied. After the autofocusing operation, a series of optical experiments using random illumination patterns with 128×128 pixels are conducted at a full sampling ratio, i.e., $N$=16384.

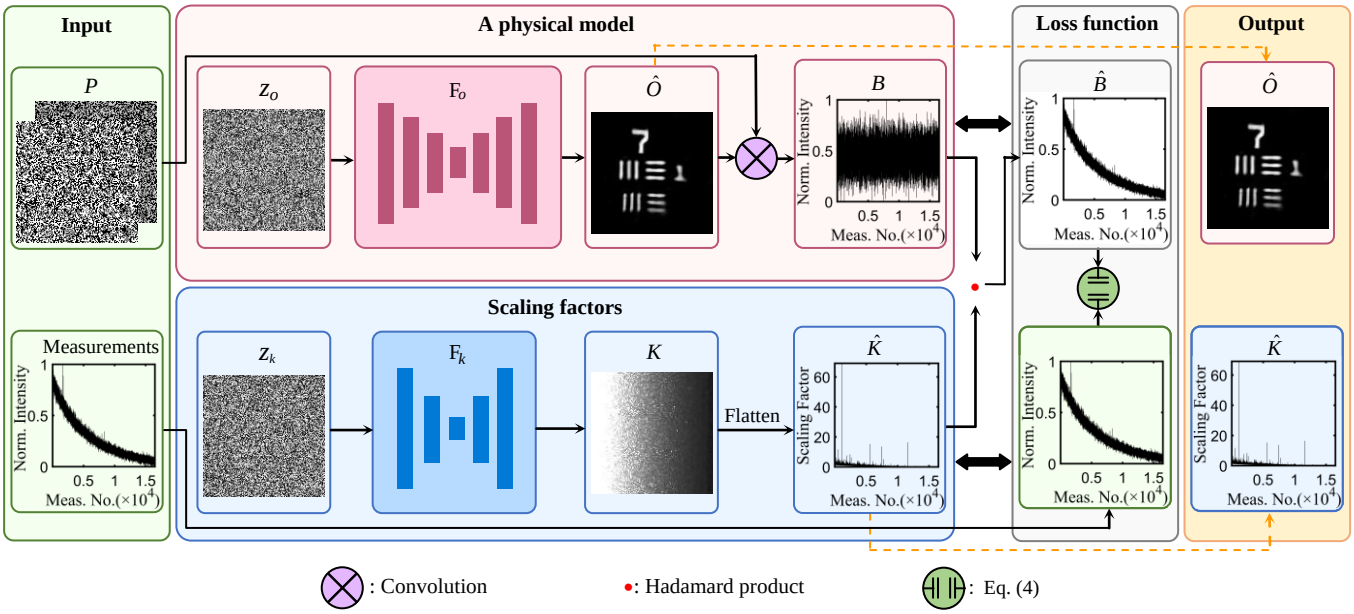


**FIG. 2.** A flow chart of the proposed physics-enhanced UNN through complex scattering media. Inputs: random illumination patterns and the measurements. Outputs: an estimated object image and a series of dynamic scaling factors.

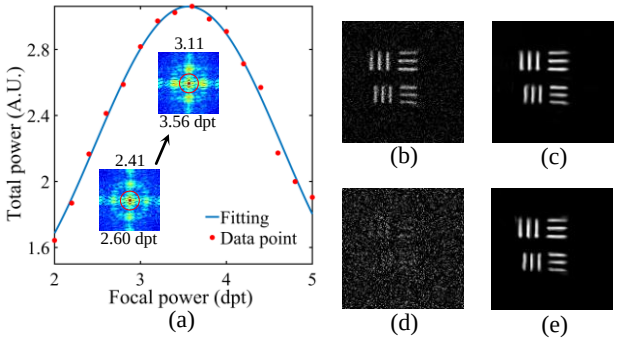


**FIG. 3.** Experimental results: (a) an illustration of the determination of focal positions, a reconstructed object image (128×128 pixels) obtained by using (b) and (d) DGI, and (c) and (e) the proposed method. (b), (c): only static and clean water placed in the optical path; (d), (e): complex scattering media in Fig. 1. Here, Group 7 Elements 5-6 of USAF 1951 resolution test chart is tested, and a line width of 2.19 μm is resolved.

As can be seen in Figs. 3(b)–3(e), when only static and clean water is placed in the optical path, DGI can be applied to reconstruct an object image and quality of the recovered object image using the proposed method is higher. In a complex scattering environment as shown in Fig. 1, DGI is ineffective. Using the proposed method, the reconstructed object image is of high quality, and high spatial resolution of 4.38 μm is achieved.

The varying scattering is further investigated by adjusting the stirring speed and the volumes of milk used in the milk suspension. The typical experimental results obtained by using DGI and the proposed method are shown in Figs. 4(a)–4(d). To quantitatively evaluate the quality, contrast-to-noise ratio (CNR)[42] is calculated as described by

$$\mathrm{CNR} = \frac{2\left|\bar{I}_s - \bar{I}_b\right|}{\sigma_s + \sigma_b}, \tag{5}$$

where $\bar{I}_s$ denotes an average intensity in a signal area of the reconstructed object image, $\bar{I}_b$ denotes an average intensity in a background area of the reconstructed object image, and $\sigma_s$ and $\sigma_b$ denote standard deviations. Figures 4(e) and 4(f) show CNR variations as different stirring speeds and different volumes of milk are employed, respectively. High-resolution object images can always be reconstructed in dynamic and complex environments, showing high effectiveness and robustness of the proposed method. To further evaluate turbidity in Fig. 1, attenuation coefficient is calculated based on Beer-Lambert law.[43,44] For instance, when 5.0-ml and 15.0-ml milk is individually used in our experiments, attenuation coefficients change from ~0 to $2.4\times10^{-2}$ $\mathrm{mm}^{-1}$ and from ~0 to $6.5\times10^{-2}$ $\mathrm{mm}^{-1}$, respectively.

Here, biological samples are also tested in Fig. 1, and their high transparency characteristics and weak intensity fluctuations make object reconstruction complicated in complex scattering environments. To verify feasibility and robustness of the proposed method in such harsh scenarios, experimental results are obtained as shown in Fig. 5. DGI still shows poor performance even when only static and clear water is placed in the optical path, and completely fails in complex environments. When the proposed method is applied, high-quality object reconstruction is always achieved.

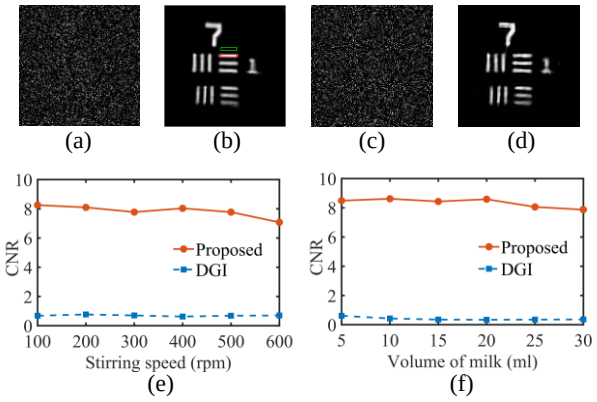


**FIG. 4.** The reconstructed object images (128×128 pixels) obtained with a stirring speed of 400 rpm and 5.0-ml of milk adopted in experiments using (a) DGI and (b) the proposed method, the reconstructed object images (128×128 pixels) obtained with a stirring speed of 450 rpm and 15.0-ml milk adopted in experiments using (c) DGI and (d) the proposed method, and the CNR curves obtained when (e) different stirring speeds with 5.0-ml milk and (f) different volumes of milk with 450 rpm stirring speed are individually used in experiments. For CNR calculations, a signal area (red box) and a background area (green box) are indicated in (b).

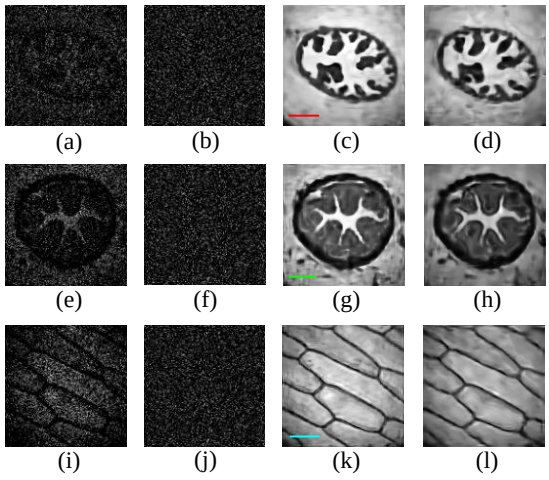


**FIG. 5.** Experimental results (biological specimens): (a)–(d) Oviduct T.S., (e)–(h) Ureter C.S. and (i)–(l) Onion Epidermis W.M. The experimental results (128×128 pixels) in the first two columns are obtained by using DGI, and the experimental results (128×128 pixels) in the last two columns are obtained by using the proposed method. Only static and clean water in Fig. 1: (a), (c), (e), (g), (i), (k); Complex scattering media in Fig. 1: (b), (d), (f), (h), (j), (l). Here, 3.0-ml milk is used, when imaging through complex media is conducted. Scale bars in (c), (g) and (k): 300 μm (red), 200 μm (green), 100 μm (blue).

In conclusion, we have reported UNN enhanced by a physical model with the designed optical setup to implement high-resolution single-pixel microscopy through complex scattering media. A series of dynamic scaling factors are accurately estimated to obtain the corrected measurements for object reconstruction. The experimental results demonstrate that the proposed method can overcome the challenge induced by dynamic and complex scattering, and high-resolution object images can be robustly recovered over the varying FOVs. It is believed that the proposed method is promising for high-resolution optical microscopic imaging through thick, dynamic and complex scattering media.

This work was supported by Hong Kong Research Grants Council General Research Fund (15224921, 15223522, 15237924), Hong Kong Research Grants Council Collaborative Research Fund (C5047-24G), and The Hong Kong Polytechnic University (1-CDJA, 1-WZ4M).

## AUTHOR DECLARATIONS

### Conflict of Interest

The authors have no conflicts to disclose.

### Author Contributions

**Tianshun Zhang:** Data curation (lead); Formal analysis (lead); Investigation (lead); Methodology (lead); Writing – original draft (lead). **Yang Peng:** Formal analysis (lead); Investigation (lead). **Wen Chen:** Conceptualization (lead); Formal analysis (lead); Methodology (lead); Project administration (lead); Supervision (lead); Writing – review & editing (lead).

## DATA AVAILABILITY

The data that support the findings of this study are available from the corresponding author upon reasonable request.

## REFERENCES

1. F. Wang, Y. Zhong, O. Bruns, Y. Liang, and H. Dai, "In vivo NIR-II fluorescence imaging for biology and medicine," Nat. Photonics **18**, 535–547 (2024).
2. F. O. Fahrbach, P. Simon, and A. Rohrbach, "Microscopy with self-reconstructing beams," Nat. Photonics **4**, 780–785 (2010).
3. T. Wu, Y. Baek, F. Xia, S. Gigan, and H. B. de Aguiar, "Replica-assisted super-resolution fluorescence imaging in scattering media," ACS Photonics **12**, 1308–1315 (2025).
4. N. Radwell, K. J. Mitchell, G. M. Gibson, M. P. Edgar, R. Bowman, and M. J. Padgett, "Single-pixel infrared and visible microscope," Optica **1**, 285–289 (2014).
5. Y. Wang, D. Wu, M. Yang, S. Bai, S. Huang, M. Wang, R. Liu, Z. Li, D. Li, and Y. Shen, "Microscopic single-pixel polarimetry for biological tissue," Appl. Phys. Lett. **122**, 203701 (2023).
6. M. Yao, Z. Cai, X. Qiu, S. Li, J. Peng, and J. Zhong, "Full-color light-field microscopy via single-pixel imaging," Opt. Express **28**, 6521–6536 (2020).

7. S.-C. Chen, Z. Feng, J. Li, W. Tan, L.-H. Du, J. Cai, Y. Ma, K. He, H. Ding, and Z.-H. Zhai, "Ghost spintronic THz-emitter-array microscope," Light Sci. Appl. **9**, 99 (2020).
8. L. Uguen, R. Piedevache, G. Russias, S. Helmer, D. Tregoat, and S. Perrin, "Single-pixel-based hyperspectral microscopy," Appl. Phys. Lett. **125**, 071108 (2024).
9. X.-H. Zhu, Y.-F. Bai, W. Tan, X.-Q. Liang, Q. Zhou, J. Li, W.-J. Zhou, J.-T. Zhai, X.-W. Huang, X.-W. Cai, and X.-Q. Fu, "Live cell imaging and classification via microscopic ghost imaging," Phys. Rev. Appl. **23**, 054018 (2025).
10. Y.-N. Zhao, L. Wang, H. Li, C. Liu, L. Guan, D.-Z. Cao, H.-C. Liu, and S.-H. Zhang, "Single-pixel dual-mode microscopy for simultaneous acquisition of magnitude and wrapped phase images," Opt. Laser Technol. **182**, 112017 (2025).
11. Y. Liu, J. Suo, Y. Zhang, and Q. Dai, "Single-pixel phase and fluorescence microscope," Opt. Express **26**, 32451–32462 (2018).
12. T. Zhang, Y. Xiao, and W. Chen, "Single-pixel microscopic imaging through complex scattering media," Appl. Phys. Lett. **126**, 031106 (2025).
13. Z. Zhang, X. Wang, G. Zheng, and J. Zhong, "Hadamard single-pixel imaging versus Fourier single-pixel imaging," Opt. Express **25**, 19619–19639 (2017).
14. Z. Sun, F. Tuitje, and C. Spielmann, "Toward high contrast and high-resolution microscopic ghost imaging," Opt. Express **27**, 33652–33661 (2019).
15. X.-H. Zhu, Y.-F. Bai, W. Tan, L.-Y. Zhou, X.-W. Huang, T.-J. Jiang, T. Jiang, S.-Q. Nan, and X.-Q. Fu, "High-resolution microscopic ghost imaging for bioimaging," Phys. Rev. Appl. **20**, 014028 (2023).
16. X. Wen, S. Adhikari, C. L. Cortes, D. J. Gosztola, S. K. Gray, and G. P. Wiederrecht, "Ghost imaging second harmonic generation microscopy," Appl. Phys. Lett. **116**, 191101 (2020).
17. N. N. Davletshin, A. M. Vyunishev, and A. S. Chirkin, "Ghost imaging microscopy: Towards to three dimensional extended depth-of-field imaging," Opt. Laser Technol. **184**, 112465 (2025).
18. S. Ota, R. Horisaki, Y. Kawamura, M. Ugawa, I. Sato, K. Hashimoto, R. Kamesawa, K. Setoyama, S. Yamaguchi, and K. Fujiu, "Ghost cytometry," Science **360**, 1246–1251 (2018).
19. H. Li, W. Hou, Z. Ye, T. Yuan, S. Shao, J. Xiong, T. Sun, and X. Sun, "Resolution-enhanced x-ray ghost imaging with polycapillary optics," Appl. Phys. Lett. **123**, 141101 (2023).
20. Y. Hao, Y. Xiao, and W. Chen, "Single-pixel imaging through random media with automated adaptive corrections," Appl. Phys. Lett. **126**, 131105 (2025).
21. Q. Song, Q. H. Liu, and W. Chen, "Ghost imaging through abruptly changing complex scattering in dynamic media," Opt. Lett. **50**, 3010–3013 (2025).
22. Z. Wang, T. Zhang, Y. Xiao, Z. Liu, and W. Chen, "Common-path ghost imaging through complex media with dual polarization," Opt. Lett. **50**, 1152–1155 (2025).
23. Y. Xiao, L. Zhou, and W. Chen, "High-resolution ghost imaging through complex scattering media via a temporal correction," Opt. Lett. **47**, 3692–3695 (2022).
24. Y. Rivenson, Z. Göröcs, H. Günaydin, Y. Zhang, H. Wang, and A. Ozcan, "Deep learning microscopy," Optica **4**, 1437–1443 (2017).
25. E. Nehme, L. E. Weiss, T. Michaeli, and Y. Shechtman, "Deep-STORM: super-resolution single-molecule microscopy by deep learning," Optica **5**, 458–464 (2018).
26. H. Pinkard, Z. Phillips, A. Babakhani, D. A. Fletcher, and L. Waller, "Deep learning for single-shot autofocus microscopy," Optica **6**, 794–797 (2019).
27. Y. Wu, Y. Rivenson, H. Wang, Y. Luo, E. Ben-David, L. A. Bentolila, C. Pritz, and A. Ozcan, "Three-dimensional virtual refocusing of fluorescence microscopy images using deep learning," Nat. Methods **16**, 1323–1331 (2019).
28. L. Hu, S. Hu, W. Gong, and K. Si, "Image enhancement for fluorescence microscopy based on deep learning with prior knowledge of aberration," Opt. Lett. **46**, 2055–2058 (2021).
29. M. Guo, Y. Wu, C. M. Hobson, Y. Su, S. Qian, E. Krueger, R. Christensen, G. Kroeschell, J. Bui, and M. Chaw, "Deep learning-based aberration compensation improves contrast and resolution in fluorescence microscopy," Nat. Commun. **16**, 313 (2025).
30. K. Song, Y. Bian, D. Wang, R. Li, K. Wu, H. Liu, C. Qin, J. Hu, and L. Xiao, "Advances and Challenges of Single-Pixel Imaging Based on Deep Learning," Laser Photonics Rev. **19**, 2401397 (2024).
31. C. F. Higham, R. Murray-Smith, M. J. Padgett, and M. P. Edgar, "Deep learning for real-time single-pixel video," Sci. Rep. **8**, 2369 (2018).
32. B. Neyshabur, S. Bhojanapalli, D. McAllester, and N. Srebro, "Exploring generalization in deep learning," Proceedings of the 31st International Conference on Neural Information Processing Systems, 5949–5958 (2017).
33. J. Wu, K. Liu, X. Sui, and L. Cao, "High-speed computer-generated holography using an autoencoder-based deep neural network," Opt. Lett. **46**, 2908–2911 (2021).
34. F. Wang, C. Wang, M. Chen, W. Gong, Y. Zhang, S. Han, and G. Situ, "Far-field super-resolution ghost imaging with a deep neural network constraint," Light Sci. Appl. **11**, 1 (2022).
35. Y. Peng and W. Chen, "Ghost imaging through complex scattering media with random light disturbance," Appl. Phys. Lett. **126**, 011108 (2025).
36. F. Ferri, D. Magatti, L. Lugiato, and A. Gatti, "Differential ghost imaging," Phys. Rev. Lett. **104**, 253603 (2010).
37. Y. Gandelsman, A. Shocher, and M. Irani, "" Double-DIP": unsupervised image decomposition via coupled deep-image-priors," in *Proceedings of the IEEE/CVF conference on computer vision and pattern recognition*, 11026–11035 (2019).
38. Z. Deng, S. Qi, Z. Zhang, and J. Zhong, "Autofocus Fourier single-pixel microscopy," Opt. Lett. **48**, 6076–6079 (2023).
39. G. Wang, H. Deng, Y. Cai, M. Ma, X. Zhong, and X. Gong, "Grating-free autofocus for single-pixel microscopic imaging," Photonics Res. **12**, 1313–1321 (2024).
40. H. Tobón-Maya, S. I. Zapata-Valencia, L. Willstatter, S. Bonora, A. Farina, J. Lancis, and E. Tajahuerce, "Autofocusing method for active Hadamard single-pixel microscopy using gradient descent algorithms," Opt. Lasers Eng. **185**, 108699 (2025).
41. H. Chen, Y. Chen, D. Shi, R. Jiang, Z. Guo, and Y. Wang, "Complementary differential detection for fast focusing using dual single-pixel detectors," Opt. Lett. **50**, 3285–3288 (2025).
42. B. Redding, M. A. Choma, and H. Cao, "Speckle-free laser imaging using random laser illumination," Nat. Photonics **6**, 355–359 (2012).
43. Y. Peng, Y. Xiao, and W. Chen, "High-fidelity optical wireless transmission in complex environments around a corner using the design of a single-layer neural network for data encoding," Opt. Express **33**, 30123–30135 (2025).
44. R. Joshi, G. Krishnan, T. O'Connor, and B. Javidi, "Signal detection in turbid water using temporally encoded polarimetric integral imaging," Opt. Express **28**, 36033–36045 (2020).